Special Double Issue Article

Yu Zhao*, Deepam Maurya, Andrew Miner, Giti A. Khodaparast and Shashank Priya

Enhanced Thermoelectric Performance in PbTe–PbS Nanocomposites

Abstract: In this study, we investigate the changes occurring in the microstructure and thermoelectric properties of $PbTe_{0.9}S_{0.1}$ alloy (PbTe–PbS) under varying thermal treatment conditions. Transmission electron microscopy (TEM) studies were utilized to reveal the distribution of nano-precipitates in the annealed alloy. $PbTe_{0.9}S_{0.1}$ alloy with PbS phase precipitates displayed a significant reduction in the thermal conductivity and an enhancement in the Seebeck coefficient. The 47% reduction in lattice thermal conductivity at the measurement temperature of 300°C in the alloy annealed at 400°C was attributed to the phonon scattering occurring due to the presence of nano-precipitates. The annealed alloy displayed higher electrical conductivity at room temperature than that of the alloy without annealing. The maximum figure of merit, *ZT*, was found to be 0.76 at 300°C in the alloy annealed at 400°C.

Keywords: thermoelectric, nano-precipitates, thermal conductivity, electrical property

DOI 10.1515/ehs-2015-0004

Introduction

Thermoelectric (TE) materials have recently attracted great attention in application for harvesting the wasted thermal energy. The efficiency of thermoelectric energy harvesting devices depends on the materials' figure of merit (*ZT*) in the given temperature regime. The prominent TE material, such as Bi_2Te_3, shows good *ZT* around room temperature, and PbTe has promising *ZT* in the temperature range of 300 to 400°C (Poudel et al. 2008; Hsu et al. 2004). However, the values of *ZT* in these materials are still low for large-scale practical application. Recently, significant efforts have been placed on the investigation of nanostructures in semiconducting thermoelectric alloys (Snyder and Toberer 2008; Vineis et al. 2010). In order to reduce the thermal conductivity effectively, nanoscale structures combined with long-wavelength phonon scattering centers (mesoscale grain/phase boundaries) and short-wavelength phonon scattering centers (atomic-scale dislocation/strain/point defects) have been found to be relevant (Wu et al. 2014).

The nano-precipitates are effective in blocking the propagation of mid-to-long-wavelength phonons hence causing the reduction in the lattice thermal conductivity (κ_{latt}). PbTe-based material systems, such as LASTT ($AgPb_mSn_nSbTe_{2+m+n}$) and SALT ($NaPb_mSbTe_{2+m}$), consisting of nanoparticles have been found to provide reduction in thermal conductivity supporting the hypothesis that phonon scattering is facilitated due to the presence of nanoparticles (Hsu et al. 2004; Guéguen et al. 2009). Nanostructure formation in PbTe matrix has been extensively investigated in recent years with the addition of modifiers such as Sb (Sootsman et al. 2008; Guéguen et al. 2009; He et al. 2010), Bi (BiSb) (Guéguen et al. 2009; He et al. 2010; Androulakis et al. 2006), Pb (Sootsman et al. 2008; He et al. 2010), SnTe (He et al. 2009), and Ag_2Te (Pei et al. 2011). In some of these PbTe-based alloys, a spontaneous decomposition occurs resulting in the growth of secondary phase precipitates with the dimension in the range of a few nanometers to 50 nm, which is in the order of magnitude the free mean path in PbTe (19 nm) (Koh et al. 2009). The compositional difference of nanoparticles from matrix results in lattice misfit dislocations or localized strain fields (large acoustic impedance mismatch/roughness).

PbTe–PbS is one of the well-known binary systems, which exhibits the miscibility gap vulnerable to thermodynamic phase separation through metastable nucleation

***Corresponding author: Yu Zhao,** Bio-inspired Materials and Devices Laboratory (BMDL), Center for Energy Harvesting Materials and Systems (CEHMS), Virginia Tech, Blacksburg, VA 24061, USA, E-mail: zhaoyu@vt.edu
Deepam Maurya, Bio-inspired Materials and Devices Laboratory (BMDL), Center for Energy Harvesting Materials and Systems (CEHMS), Virginia Tech, Blacksburg, VA 24061, USA, E-mail: mauryad@vt.edu
Andrew Miner, Romny Scientific Inc., San Bruno, CA 94066, USA, E-mail: miner@romny-scientific.com
Giti A. Khodaparast, Physics Department, Virginia Tech, Blacksburg, VA 24061, USA, E-mail: khoda@vt.edu
Shashank Priya, Bio-inspired Materials and Devices Laboratory (BMDL), Center for Energy Harvesting Materials and Systems (CEHMS), Virginia Tech, Blacksburg, VA 24061, USA, E-mail: spriya@vt.edu

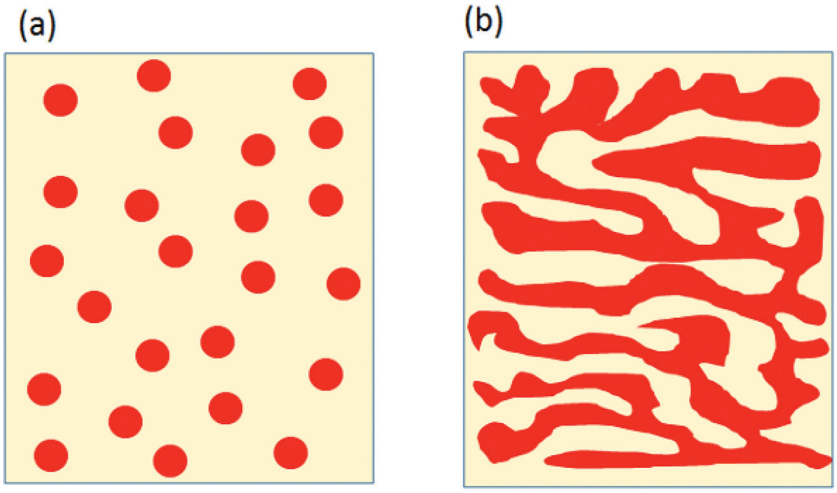

Figure 1: Schematic structure from (a) nucleation and growth process and (b) spinodal decomposition.

and growth or spinodal decomposition process (Girard et al. 2013; Liu and Chang 1994), achieving two different nanostructures as schematically shown in Figure 1. The nucleation and growth region is generally found at the outer extremes of the composition range where free energy curve has positive curvature suggesting even small variation in composition may result in enhanced free energy (Girard et al. 2013). When the system is cooled rapidly, it assumes the metastable phase. In this case, the free energy of the system can be decreased by forming nuclei that has a different composition during subsequent heat treatment. These nuclei further grow by using downhill diffusion. The spinodal decomposition starts in the inner regime of the phase diagram having negative curvature in free energy curve where small compositional variation can reduce the free energy. Consequently in this regime, the system develops small compositional fluctuations followed by coarsening via uphill diffusion process (Girard et al. 2013). In comparison to the thin films with quantum dot superlattices and bulk materials with nanograins, the nano-precipitates or laminated nanostructure in bulk TE materials have the listed advantages: (i) the synthesis process is thermodynamically driven and the variables can be adjusted using the well-established phase diagram and (ii) the structures are stable below the phase transformation temperature as the process results in the reduction of Gibbs energy, thus allowing high degree of repeatability.

These nanostructures vary in shape and size depending upon the composition and temperature of heat treatment (Girard et al. 2013). The nucleation and growth of nano-precipitates (size < 50 nm) has been observed in the PbTe system containing PbS in the range of 4–16% (Androulakis et al. 2007). The composition PbTe with 16% PbS has been found to exhibit laminated structure with the period of oscillation about 2 nm (Androulakis et al. 2007). For different amounts of PbS in PbTe matrix, the temperature of the phase separation was found to vary in the range of 500–800°C (Liu and Chang 1994). According to the phase diagram of PbS–PbTe (Liu and Change 1994), the composition $(PbTe)_{0.9}(PbS)_{0.1}$ has a decomposition boundary around 500°C. Different annealing conditions are expected to result in varying microstructural changes and dispersion in the PbTe–PbS alloy as the transformation energy is temperature dependent.

For thermoelectric materials, the power factor is an important parameter given by the product of Seebeck coefficient (α) and electrical conductivity (σ). Both α and σ are related to carrier density; however, their trends of variations are opposite (Snyder and Toberer 2008; Chen et al. 2003). Besides, the enhancement in α can be achieved by increasing the density of states over Fermi energy without deteriorating electrical conductivity. Hermans et al. have reported that a distortion (resonant levels close to the Fermi level) in the electronic density of states by doping Tl element enhances the Seebeck coefficient (Heremans et al. 2008). In PbTe–PbS system, the S atom stays in two phases after phase transformation: PbTe matrix and PbS phase. Depending upon the site occupancy of S atom in the lattice, the electrical properties of the material will be different. The PbS precipitates in PbTe matrix are expected to influence the charge carrier scattering in addition to the modulated band structure due to the sulfur in the PbTe lattice. These variations consequently change the electrical conductivity and Seebeck coefficient of PbTe. However, the effects of S atoms in matrix or in secondary phase on the electrical properties are still not well quantified. In this study,

we focus on the phase separation occurring in the $PbTe_{0.9}PbS_{0.1}$ composition on cooling down the system (Liu and Chang 1994). The impact of annealing treatment on nanostructure and thermoelectric properties was measured and utilized to develop the structure–property relationship.

Experimental

Bulk $PbTe_{0.9}S_{0.1}$ alloy was synthesized by mixing and melting Pb (100 mesh, purity 99.95%, Alfa Aesar), Te (60 mesh, purity 99.999%, Alfa Aesar), and PbS (purity 99.9%, Alfa Aesar) as starting components with 0.055% PbI_2 (purity 99.9985%, Alfa Aesar) as dopant. The mixtures were kept in a graphite crucible sealed in a quartz tube under high vacuum 10^{-6} Torr (1.3332×10^{-4} Pascal). The mixed powders were melted into liquid phase using an inductive furnace for 2 min, and then rapidly cooled down to room temperature under Ar gas flow. Next, the alloy samples were annealed at 400 and 500°C under 10^{-6} Torr vacuum for two days. Here after we term the alloy samples annealed at 400 and 500°C as PbTe–PbS-400 and PbTe–PbS-500 respectively. The rapidly cooled sample of $PbTe_{0.9}S_{0.1}$ is referred as PbTe–PbS.

To confirm the formation of phase, XRD were recorded at room temperature using X-ray diffractometer (XRD, PANalytical X'Pert, CuKa; Philips, Almelo, the Netherlands). The electrical resistivity was measured by the van der Pauw method, while Seebeck coefficient was determined using change in voltage with respect to change in the temperature under Argon. The Hall Effect measurements were conducted in the van der Pauw geometry to determine the carrier density. The thermal conductivity was determined through thermal diffusivity measurement using Xenon flash technique. The electronic contribution to the total thermal conductivity was calculated using the Wiedemann–Franz law, $\kappa_{elec} = \sigma TL$ (where σ is the electrical conductivity, T is the temperature, and L is 2.45×10^8 $W\Omega K^2$ for degenerate semiconductors). The lattice component κ_{latt} was then calculated using the relation $\kappa_{latt} = \kappa_{tot} - \kappa_{elec}$. TEM investigations were carried out using JEOL 2100 transmission electron microscope. TEM samples were prepared using the conventional polishing and grinding technique followed by the ion milling.

Results and Discussion

PbTe has a rocksalt type structure with Cubic symmetry (Fm-3m, Z=4). Both Pb and Te atoms are in fixed positions at ½½½ and 000 respectively with octahedral coordination (Stojanovic 2006). The ionic radii of Pb^{2+} and Te^{2-} atoms in *6-fold* coordination are 1.19 Å and 2.21 Å, respectively. However, the ionic radius of smaller S atom in *6-fold* coordination is 1.84 Å. The schematic of the unit cell for PbTe and substituted PbS is shown in Figure 2. The Pauling electronegativity values of Pb, Te and S are 2.33, 2.1 and 2.58 respectively. The large difference in ionic radii and electronegativity of substituted S atoms on Te sites destabilize the system by increasing the free energy. The precipitation of PbS can be further understood by assuming the ionic bond strength (IAB) using Pauling's equation: $I_{AB} = 1 - \exp\left[-\frac{X_A - X_B}{4}\right]$, where X_A and X_B is the electronegativity of cation A and anion B (Singh, Acharya, and Bhoga 2006). The ionic bond strength of Pb-S bond is ~0.06, which is slightly higher than that of Pb-Te ~0.05. We believe that these differences play a major role toward limited solubility of PbS in PbTe matrix facilitating the precipitation of PbS in PbTe matrix. In present work, the optimized thermal treatment of $PbTe_{0.9}S_{0.1}$ system resulted in PbS precipitates distributed in the PbTe matrix. Under rapid cooling, the sulfur and lead atoms did not have enough time to nucleate and precipitate. Further, the alloy samples were annealed at the temperatures in the immiscible region just below the boundary for the phase transformation.

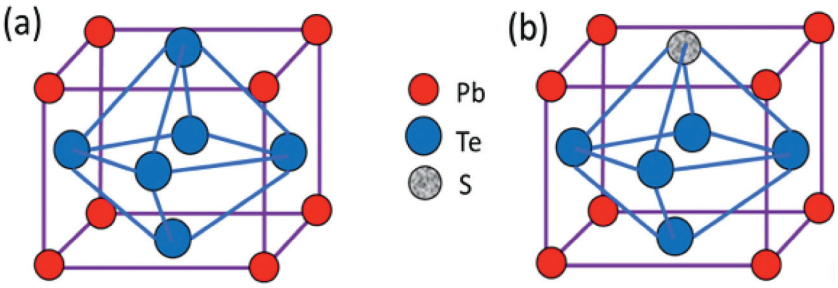

Figure 2: Schematic illustration of the unit cell of (a) PbTe (b) S substituted PbTe.

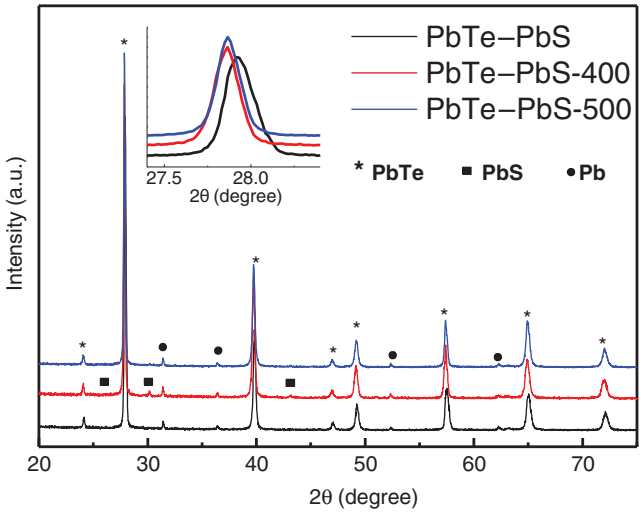

Figure 3: XRD results of as-quenched PbTe–PbS alloy and after two-day annealing; the inset is zoomed-in vision of the data.

The XRD results (Figure 3) were recorded from the ground alloy powders before and after the thermal treatment. These XRD diffractogram confirm the formation of PbTe phase in all samples. After annealing the sample at 400°C, one can observe the PbS phase as secondary phase. No obvious reflections from PbS were observed in the XRD diffractogram from the alloy annealed at 500°C suggesting the presence of significantly small amount of PbS. Prior studies have shown that after annealing at 500°C, the existence of PbS in PbTe–8% PbS was not visible through conventional XRD (Androulakis et al. 2007). At temperature >500°C, the PbS was found to dissolve in the matrix of PbTe–8% PbS (Girard et al. 2013). The precipitation of PbS was evidenced by a shift in the major PbTe reflections toward the lower value of 2θ (Girard et al. 2010), as shown in the inset of Figure 3. The lattice parameters increased in PbTe alloy after annealing due to precipitation of PbS from PbTe matrix. All specimens were found to contain a small amount of Pb phase due to Te-deficient system as a result of the relatively low evaporation temperature ~988°C of Te (slightly higher than the melting temperature of PbTe ~924°C). Since all alloys had a small amount of Pb phase, it was assumed to have relatively similar effect on the thermoelectric properties.

In order to investigate the microstructure of PbTe–PbS-400, high-resolution transmission electron microscopy was performed. Figure 4(a) shows the homogeneously distributed nano-precipitates (≤5 nm) in the PbTe matrix. The high-resolution TEM image of a larger precipitate (10 × 20 nm) is shown in Figure 4(b). A series of dislocations were observed. The PbTe and PbS have about 6% of the lattice mismatch at room temperature, which can result in considerable lattice strain at the PbTe/PbS boundaries giving rise to misfit dislocations. Furthermore, as observed from this HR-TEM image, the orientation of the precipitate (please see FFT patterns from the matrix and precipitate) is different from that of the matrix, suggesting semi-coherent interface of the precipitate and matrix. Figure 4(c) shows the HR-TEM image of another nano-precipitate observed from the [011] zone axis. The FFT pattern corresponding to Figure 4(c) is shown in the inset. The FFT suggests coherent nature of these smaller precipitates. Therefore, it can be assumed that the system has distribution of precipitates with coherent and semi-coherent interfaces. The diffraction pattern from the precipitate and the matrix is shown in Figure 4(d). The splitting of diffracted spots appears to be originated from the cubic PbTe matrix and cubic PbS second phase. In the PbTe–PbS-400 sample, no spinodal structure was found. The nanoparticles formed by nucleation and growth have been reported to be effective in scattering phonons (Androulakis et al. 2007; Girard et al. 2010). The interface area between the precipitated phase and matrix has been expected to be larger with higher compositional contrast. However, spinodal decomposition generally exhibits small compositional difference.

Figure 5(a) displays the electrical conductivity (σ) of the melted and annealed PbTe–PbS samples. It can be seen that the electrical conductivity decreased with the temperature in the range of room temperature to 300°C. The electrical conductivity of PbTe–PbS alloy was found to decrease from 1,245.6 S/cm (at room temperature) to 559.4 S/cm (at 300°C). After annealing, PbTe–PbS-400 displayed slightly higher electrical conductivity of 1,290.2 S/cm at room temperature which was reduced to 415 S/cm at 300°C. PbTe–PbS-500 was also found to exhibit higher value of 1,578.6 S/cm at room temperature, and this magnitude decreased rapidly with increasing measurement temperature to 415 S/cm at 300°C. The results indicate that annealed alloys display higher electrical conductivity at room temperature than that of unannealed one. With increasing measurement temperature, the electrical conductivity of annealed alloy decreases faster resulting in a lower value at relatively high temperature.

The decrease in electrical conductivity as a function of measurement temperature can be explained by assuming a power law $\sigma \approx \sigma_0 T^{\alpha}$ (Sootsman et al. 2008). The exponent α extracted from the data was found to be –1.45, –1.63, and –1.96 for PbTe–PbS, PbTe–PbS-400 and PbTe–PbS-500 alloys. For the $PbTe_{0.9}S_{0.1}$ alloy, the exponent α was larger than the α of PbTe with PbS

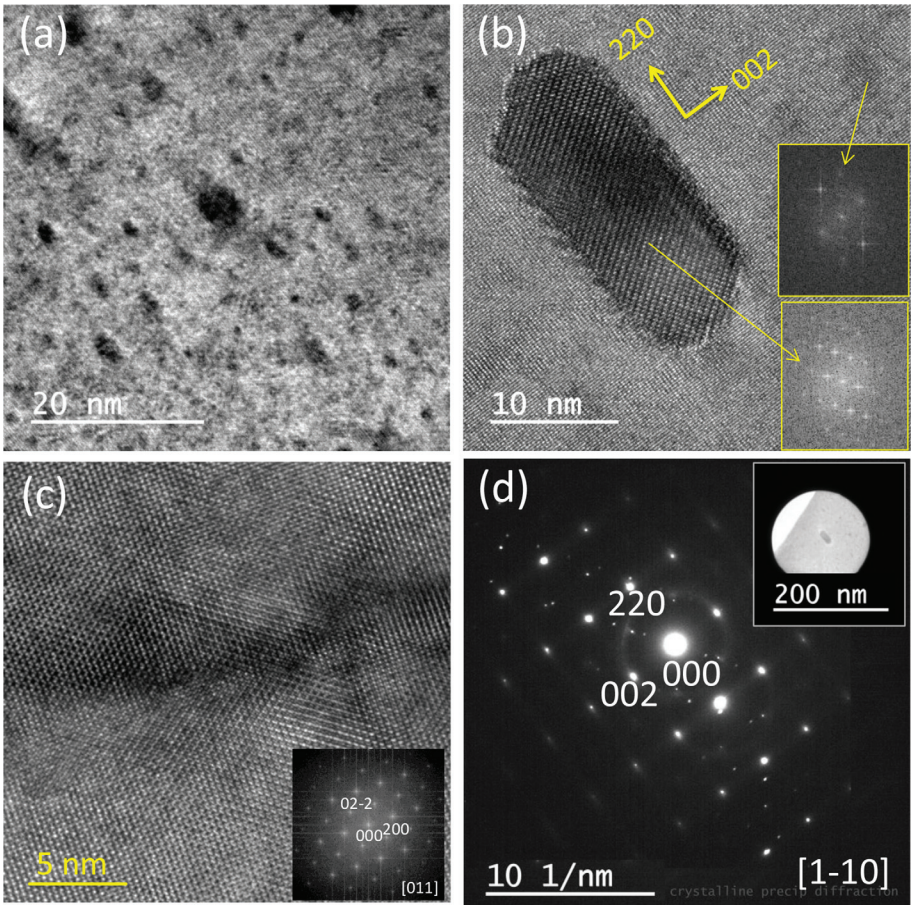

Figure 4: Characteristic TEM images of PbTe–PbS-400 (a) widely distributed nano-precipitates in the matrix; (b) high magnification TEM image showing precipitates having semi-coherent interface with PbTe matrix (the insets of (b) are FFT patterns from the precipitate and matrix); (c) high magnification TEM image showing precipitates having coherent interface with PbTe matrix (the inset of (c) is FFT patterns corresponding to Figure 4 c); and (d) electron diffraction pattern from the area of precipitate and matrix shown in the inset of (d).

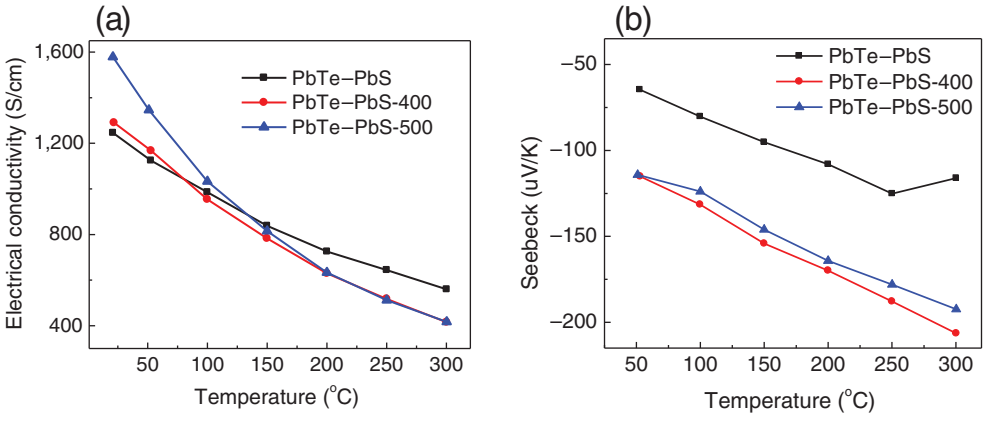

Figure 5: (a) Electrical conductivity, and (b) Seebeck coefficient of PbTe–PbS, PbTe–PbS-400, and PbTe–PbS-500 alloys.

precipitates, which indicates electrical conductivity decreased slowly with increasing measurement temperature for solid $PbTe_{0.9}S_{0.1}$. The Seebeck coefficient (Figure 5(b)) of annealed alloys was found to vary almost linearly with measurement temperature, which suggests that the carrier concentration was almost constant with temperature variation. Thereby, the power exponent α was derived from the temperature dependence of the carrier mobility, which is a function of scattering time. Electrons are scattered by the thermal vibrations of the lattice as well as precipitates in the annealed samples. The presence of nanoparticles provided additional interface for scattering, which contributes to power exponent reduction. The PbS precipitates in PbTe–PbS-500 might be small because of the small super-cooling and might be effective in scattering charge carriers.

The carrier concentration from Hall Effect measurement at room temperature was measured to be 0.99×10^{19}, 1.39×10^{19}, and 1.14×10^{19} cm^{-3} for PbTe–PbS, PbTe–PbS-400, and PbTe–PbS-500, respectively. The carrier concentration was higher in the alloy with PbS phase precipitation. The dopant PbI_2 has been previously reported to be an excellent dopant for PbTe due to the similarity in atomic radii of iodine and tellurium (Girard et al. 2010). However, it is not considered as a good dopant in PbS system because of large difference in ionic radii between iodine and sulfur (Girard et al. 2010). With less distribution of the sulfur atoms in PbS precipitates, more iodine atoms replace the tellurium to contribute free electrons in PbTe matrix.

Figure 5(b) shows the Seebeck coefficient (α) of PbTe–PbS alloys before and after annealing as a function of temperature. All the alloys exhibited negative Seebeck coefficients over the entire temperature range indicating *n*-type conduction. The annealing process greatly improved the absolute value of Seebeck coefficient. The maximum value of α at room temperature was found to be 115 μV/K for PbTe–PbS-400, which further increased almost linearly up to 206 μV/K at 300°C. This result demonstrates that precipitation of PbS that is formed inside the PbTe matrix results in an enhancement in the absolute value of the Seebeck coefficient.

The thermal conductivity (κ) of annealed PbTe–PbS alloy was smaller over the entire temperature range in comparison to that of as-melted PbTe–PbS alloy (Figure 6(a)). The κ value at 300°C was found to decrease from 2.18 W/mK for PeTe-PbS to 1.51 W/mK for PbTe–PbS-500, and 1.32 W/mK for PbTe–PbS-400, suggesting maximum 40% decrease. The κ_{latt} was calculated and was plotted in Figure 6(b). In the temperature range of measurements, a larger reduction of κ_{latt} was observed for both PbTe–PbS-400 and PbTe–PbS-500 samples, which accounted for the overall thermal conductivity reduction. The κ_{latt} value at 300°C was observed to decrease from 1.39 W/mK for PeTe-PbS to 0.92 W/mK for PbTe–PbS-500 and 0.74 W/mK for PbTe–PbS-400, achieving maximum 47% decrease. The lower lattice thermal conductivity of both PbTe–PbS-400 and PbTe–PbS-500 was attributed to the effective phonon scattering from PbS precipitation in-line with the microstructural analysis. The PbTe–PbS-400 specimen exhibited lower κ and κ_{latt} than PbTe–PbS-500 over the whole measurement temperature region. In PbTe–PbS-400 system, the driving force for secondary phase separation is larger at lower annealing temperature.

The enhanced Seebeck coefficient and the reduced thermal conductivity of annealed alloys had direct impacts on the thermoelectric figure of merit *ZT*, which exhibited much higher value than the as-melted alloy (Figure 7). PbTe–PbS-500 exhibited ZT value up to 0.59 at 300°C, whereas PbTe–PbS-400 was found to display

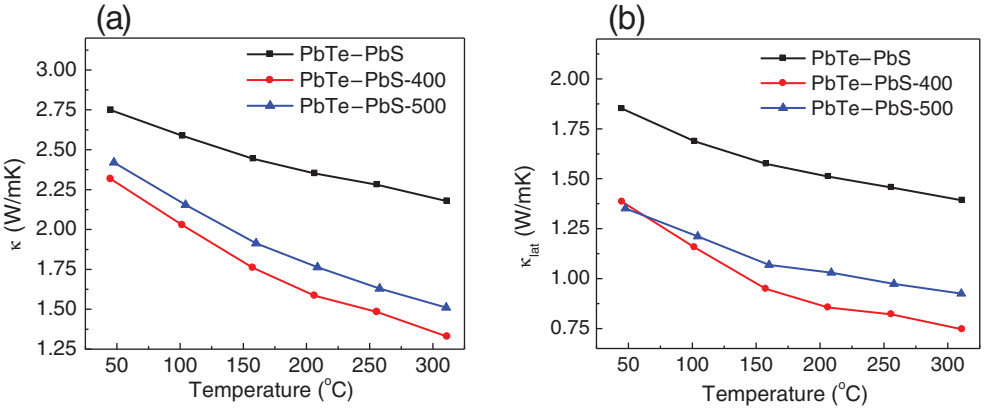

Figure 6: (a) Thermal conductivity and (b) lattice thermal conductivity of PbTe–PbS, PbTe–PbS-400, and PbTe–PbS-500 alloys.

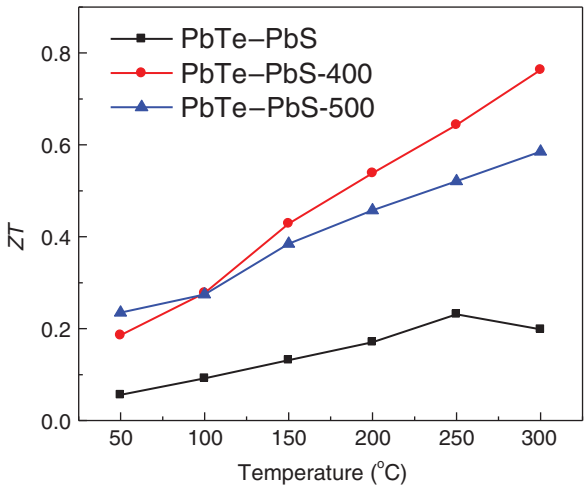

Figure 7: Figure of merit for the PbTe–PbS, PbTe–PbS-400, and PbTe–PbS-500 alloys.

higher ZT value of ~0.76 at 300°C. This ZT value was more than three times higher than that of PbTe–PbS.

Conclusions

In summary, we have studied the thermal treatment effect on $PbTe_{0.9}PbS_{0.1}$ alloys and developed correlation between the microstructures and thermoelectric behavior. The annealed alloys were found to exhibit precipitate microstructure driven by the nucleation and growth occurring in the immiscible regime of the phase diagram. After heat treatment, alloys displayed higher electrical conductivity than that of the as-melted alloy at room temperature. The precipitation of PbS was found to enhance the carrier concentration in the system. With increasing measurement temperature, the decrease in electrical conductivity was faster due to the decreased mobility of the charge carriers. The lower value of the thermal conductivity 1.32 W/mK was achieved in PbTe–PbS-400 alloy at 300°C as a result of strong phonon scattering due to the nano-precipitates. These concomitant effects resulted in three times enhanced ZT ~ 0.76 at 300°C for PbTe–PbS-400 sample.

Acknowledgments: Authors (Y.Z. and D.M.) gratefully acknowledge the financial support provided by Institute for Critical Technology and Applied Science (ICTAS) and Center for Energy Harvesting Materials and Systems (CEHMS). S.P. acknowledges the financial support from the NSF–DOE partnership on thermoelectric materials. Y.Z. would like to thank Christopher Winkler for the help with TEM analysis.

References

Androulakis, J., K. F. Hsu, R. Pcionek, H. Kong, C. Uher, J. J. D'Angelo, A. Downey, T. Hogan, and M. G. Kanatzidis. 2006. "Nanostructuring and High Thermoelectric Efficiency in p-Type $Ag(Pb_{1-y}Sn_y)_mSbTe_{2+m}$." *Advanced Materials* 18: 1170.

Androulakis, J., C. H. Lin, H. J. Kong, C. Uher, C. I. Wu, T. Hogan, B. A. Cook, T. Caillat, K. M. Paraskevopoulos, and M. G. Kanatzidis. 2007. "Spinodal Decomposition and Nucleation and Growth as a Means to Bulk Nanostructured Thermoelectrics: Enhanced Performance in $Pb_{(1-x)}Sn_{(x)}Te$-PbS." *Journal of the American Chemical Society* 129: 9780.

Chen, G., M. S. Dresselhaus, G. Dresselhaus, J. P. Fleurial, and T. Caillat. 2003. "Recent Developments in Thermoelectric Materials." *International Materials Reviews* 48: 45.

Girard, S. N., J. He, C. Li, S. Moses, G. Wang, C. Uher, V. P. Dravid, and M. G. Kanatzidis. 2010. "In Situ Nanostructure Generation and Evolution Within a Bulk Thermoelectric Material to Reduce Lattice Thermal Conductivity." *Nano Letters* 10: 2825.

Girard, S. N., K. Schmidt-Rohr, T. C. Chasapis, E. Hatzikraniotis, B. Njegic, E. M. Levin, A. Rawal, K. M. Paraskevopoulos, and M. G. Kanatzidis. 2013. "Analysis of Phase Separation in High Performance PbTE-PbS Thermoelectric Materials." *Advanced Functional Materials* 23: 747.

Guéguen, A., P. F. P. Poudeu, C. P. Li, S. Moses, C. Uher, J. Q. He, V. Dravid, K. M. Paraskevopoulos, and M. G. Kanatzidis. 2009. "Thermoelectric Properties and Nanostructuring in the p-Type Materials $NaPb_{18-x}Sn_xMTe_{20}$ (M = Sb, Bi)." *Chemistry of Materials*: 21: 1683–94.

He, J. Q., A. Gueguen, J. R. Sootsman, J. C. Zheng, L. J. Wu, Y. M. Zhu, M. G. Kanatzidis, and V. P. Dravid. 2009. "Role of Self-Organization, Nanostructuring, and Lattice Strain on Phonon Transport in $NaPb_{18-x}Sn_xBiTe_{20}$ Thermoelectric Materials." *Journal of the American Chemical Society* 131: 17828.

He, J. Q., J. R. Sootsman, S. N. Girard, J. C. Zheng, J. G. Wen, Y. M. Zhu, M. G. Kanatzidis, and V. P. Dravid. 2010. "On the Origin of Increased Phonon Scattering in Nanostructured PbTE Based Thermoelectric Materials." *Journal of the American Chemical Society* 132: 8669.

Heremans, J. P., V. Jovovic, E. S. Toberer, A. Saramat, K. Kurosaki, A. Charoenphakdee, S. Yamanaka, and G. J. Snyder. 2008. "Enhancement of Thermoelectric Efficiency in PbTE by Distortion of the Electronic Density of States." *Science* 321: 554.

Hsu, K. F., S. Loo, F. Guo, W. Chen, J. S. Dyck, C. Uher, T. Hogan, E. K. Polychroniadis, and M. G. Kanatzidis. 2004. "Cubic $AgPB_{(m)}SbTE_{(2+m)}$: Bulk Thermoelectric Materials with High Figure of Merit." *Science* 303: 818.

Koh, Y. K., C. J. Vineis, S. D. Calawa, M. P. Walsh, and D. G. Cahill. 2009. "Lattice Thermal Conductivity of Nanostructured Thermoelectric Materials Based on PbTE." *Applied Physics Letters* 94: 153101.

Liu, H., and L. L. Y. Chang, "Phase Relations in the System PbTE-PbS-PbSN" *Mineralogical Magazine* 58 (1994).

Pei, Y., N. A. Heinz, A. LaLonde, and G. J. Snyder. 2011. "Combination of Large Nanostructures and Complex Band Structure for High Performance Thermoelectric Lead Telluride." *Energy & Environmental Science* 4: 3640.

Poudel, B., Q. Hao, Y. Ma, Y. Lan, A. Minnich, B. Yu, X. Yan, D. Wang, A. Muto, D. Vashaee, et al. 2008. "High-Thermoelectric

Performance of Nanostructured Bismuth Antimony Telluride Bulk Alloys." *Science* 320: 634.

Singh, K., S. A. Acharya, and S. S. Bhoga. 2006. "Nanosized Ceria-Based Ceramics: A Comparative Study." *Ionics* 12: 295.

Snyder, G. J., and E. S. Toberer. 2008. "Complex Thermoelectric Materials." *Nature Materials* 7: 105.

Sootsman, J. R., H. Kong, C. Uher, J. J. D'Angelo, C. I. Wu, T. P. Hogan, T. Caillat, and M. G. Kanatzidis. 2008. "Large Enhancements in the Thermoelectric Power Factor of Bulk PbTE at High Temperature by Synergistic Nanostructuring." *Angewandte Chemie* 47: 8618.

Stojanovic, J. N. 2006. "Structural and Microstructural Characteristics of B-Doped PbTE Semiconductor." *Journal of Minerals and Materials Characterization and Engineering* 5: 143.

Vineis, C. J., A. Shakouri, A. Majumdar, and M. G. Kanatzidis. 2010. "Nanostructured Thermoelectrics: Big Efficiency Gains From Small Features." *Advanced Materials* 22: 3970.

Wu, H. J., L. D. Zhao, F. S. Zheng, D. Wu, Y. L. Pei, X. Tong, and J. Q. He. 2014. "Understanding the Role of Potassium Doping in PbTE-PbS Thermoelectrics." *Microscopy and Microanalysis* 20: 506.